Comparative effects of zinc oxide nanoparticles and dissolved zinc on zebrafish embryos and eleuthero-embryos: Importance of zinc ions

Comparative effects of zinc oxide nanoparticles and dissolved zinc on zebrafish embryos and eleuthero-embryos: importance of zinc ions

Nadja Rebecca Brun[1,2], Markus Lenz[1,3], Bernhard Wehrli[2], Karl Fent[1,2 *]

[1] University of Applied Sciences and Arts Northwestern Switzerland, School of Life Sciences, Institute for Ecopreneurship, Gründenstrasse 40, CH-4132 Muttenz, Switzerland

[2] ETH Zurich, Institute of Biogeochemistry and Pollutant Dynamics, Universitätsstrasse 16, CH-8092 Zürich, Switzerland

[3] Wageningen University, Department of Environmental Technology, NL-6708 WG Wageningen, The Netherlands

*Corresponding author:

Prof. Dr. Karl Fent, Gründenstrasse 40, CH-4132 Muttenz, Switzerland.

E-mail: karl.fent@fhnw.ch; Tel.: +41 61 467 45 71

Abstract

The increasing use of zinc oxide nanoparticles (nZnO) and their associated environmental occurrence makes it necessary to assess their potential effects on aquatic organisms. Upon water contact, nZnO dissolve partially to zinc (Zn(II)). To date it is not yet completely understood, whether effects of nZnO are solely or partly due to dissolved Zn(II). Here we compare potential effects of 0.2, 1 and 5 mg/L nZnO and corresponding concentrations of released Zn(II) by water soluble $ZnCl_2$ to two development stages of zebrafish, embryos and eleuthero-embryos, by analysing expressional changes by RT-qPCR. Another objective was to assess uptake and tissue distribution of Zn(II). Laser ablation-ICP-MS analysis demonstrated that uptake and tissue distribution of Zn(II) was identical for nZnO and $ZnCl_2$ in eleuthero-embryos. Zn(II) was found particularly in the retina/pigment layer of eyes and brain. Both nZnO and dissolved Zn(II) derived from $ZnCl_2$ had similar inhibiting effects on hatching, and they induced similar expressional changes of target genes. At 72 hours post fertilization (hpf), both nZnO and Zn(II) delayed hatching at all doses, and inhibited hatching at 1 and 5 mg/L at 96 hpf. Both nZnO and Zn(II) lead to induction of metallothionein (*mt2*) in both embryos and eleuthero-embryos at all concentrations. Transcripts of oxidative stress related genes *cat* and *Cu/Zn sod* were also altered. Moreover, we show for the first time that nZnO exposure results in transcriptional changes of pro-inflammatory cytokines *IL-1β* and *TNFα*. Overall, transcriptional alterations were higher in embryos than eleuthero-embryos. The similarities of the effects lead to the conclusion that effects of nZnO are mainly related to the release of Zn(II).

Keywords: zinc oxide nanoparticle, gene expression, pro-inflammatory response, embryotoxicity, laser ablation bioimaging, zinc uptake

1. Introduction

Metal-based nanoparticles are increasingly implemented in materials, cosmetics and technical applications. Consequently, they may be ultimately released into the environment during production, use and disposal at the end of their life. Zinc oxide nanoparticles (nZnO) are widely used in semiconductors, (organic) solar panel devices (Zimmermann et al. 2012), paints, personal care products (sunscreens) and even in waste water treatment. Nanoparticles might have different physico-chemical properties or behaviour in contrast to bulk materials, making prediction of their fate challenging (Li et al. 2013; Li et al. 2014). Their state of aggregation, and consequently their settling to sediments, depends on surface properties, abiotic factors and presence of dissolved organic matter in surrounding media (Shaw and Handy, 2011; Zhou and Keller, 2010). Most (nano)particles in aquatic environments are covered by adsorbed layers of natural organic material, such as humic substances and polysaccharides, which can influence stability of inorganic nanoparticles suspensions (Hyung et al., 2007) and provide potential binding sites for trace elements (Buffle et al., 1990).

Zinc is an essential trace element for organisms but induces toxicity at elevated concentrations. Partially but relatively quickly, nZnO dissolve in water, and the release of free zinc ions has been previously shown to be the primary source of toxicity (Blinova et al., 2010; Buerki-Thurnherr et al., 2013; Franklin et al., 2007). However, in other studies nZnO showed higher toxicity (Bai et al., 2009; Hu et al., 2009; Fernández et al., 2013), or induced additional effects (Poynton et al., 2011) than dissolved Zn(II) alone. Thus, there are conflicting observations and therefore further research is needed to resolve these discrepancies.

In organisms, cellular zinc ion fluctuations are mainly regulated by zinc binding metallothioneins (MT). Both, Zn(II) and nZnO induce reactive oxygen species (ROS) formation (Dineley et al., 2003; Heng et al., 2010; Sensi et al., 1999). ROS induction triggering an oxidative stress response has become a widely accepted paradigm for cellular effects of nanoparticles (Nel et al., 2006; Sharma et al., 2012; Song et al., 2010; Zhu et al., 2009). Excessive production of ROS can induce pro-inflammatory and cytotoxic effects (Nel et al., 2006). nZnO and associated released Zn(II) may

ultimately lead to apoptosis (Buerki-Turnherr et al. 2013) and acute toxicity at high concentrations. In zebrafish, adverse effects of nZnO include reduced hatching of embryos and ROS production (Bai et al., 2009; George et al., 2011; Ong et al., 2013; Xia et al., 2011; Zhao et al., 2013; Zhu et al., 2009). However, induction of inflammatory responses has not yet been investigated in fish.

In our present study we compare effects of nZnO and equal concentrations of released Zn(II) (derived from $ZnCl_2$) in experimental exposures of embryos and hatched zebrafish eleuthero-embryos in environmentally relevant media. Naturally occurring alginate, a polysaccharide-based organic material, was chosen as a supplement to stabilize nanoparticles and reduce their aggregation rate (George et al., 2012, 2011). We hypothesize that effects in embryos and eleuthero-embryos are similar, because they are induced by released Zn(II). This is assumed because agglomerated nanoparticles might not pass the pores in the chorion (Fent et al., 2010), but rather act as "delivery vehicle" for zinc ions when attached to the chorion (Handy et al., 2008). The aims of our present work were to (1) evaluate the role of the protective egg chorion; (2) compare the influence of nZnO and released Zn(II); (3) determine the uptake of zinc by embryos and eleuthero-embryos using ICP-MS analysis, and its distribution into tissues by laser-ablation ICP-MS imaging; and (4) to assess the effects of nZnO and Zn(II) on the expression of target genes including pro-inflammatory genes. Our results indicate a fast dissolution of zinc from nZnO in water, making the free metal ions the primary source of the observed effects.

2. Materials and Methods

2.1 Nanoparticle characterisation

Zinc oxide nanoparticles (nZnO) were supplied by Genes'Ink (Marseille, France). The specific surface area was analysed by BET method (Brunauer et al., 1938) on a Gemini model 2380 (Micromeritics Instrument Corp., Georgia, USA). In addition, the zeta potential of nZnO in the exposure medium was measured using a Malvern Zetasizer Nano ZS (Malvern Instruments ltd., Malvern, UK). In the electric field, the electrophoretic mobility of charged nanoparticles was determined at 25°C. Automatic measurements (10-100 runs) were performed with triplicates and the Smoluchowski's model was applied for analysis.

For scanning electron microscopy (SEM; Carl Zeiss Supra 40 VP, Germany) nZnO were dispersed in H_2O, ultrasonicated for 5 minutes at a frequency of 37 kHz (Elmasonic S 30) and air dried. The working distance was set on 4 mm, and an acceleration voltage of 5 kV was used.

Mean size of single particles was determined by tracking the scattered light using the NanoSight LM10 (NanosSight Ltd., Amesbury, UK) followed by evaluation using the Nanoparticle Tracking Analysis (NTA) software. The system relies on the Brownian motion and records a multitude of particles over a period of time generating a subsequent size distribution and mean size. Each concentration of nZnO and $ZnCl_2$, as well as controls, were analysed three times independently by NTA at 0 h and 24 h after preparation. Each sample was injected three times and analysed in triplicate calculating the arithmetic average thereof. Standard deviations were determined from mean size obtained from replicate runs.

2.2 Inductively-coupled-plasma mass-spectrometry (ICP-MS)

The zinc ion dissolution of nZnO in Holtfreter's Media at 0 h and 24 h after sample preparation was quantified using ICP-MS. Samples were centrifuged for 30 min at 30'000 g and the concentrations of the zinc isotopes (using ^{64}Zn and ^{66}Zn) in the supernatant were determined using an ICP-MS system

(Agilent 7500cx, Basel, Switzerland) equipped with an Octopole Reaction System, pressurized with an optimized helium flow of 5 mL min^{-1}. Supernatants were diluted 1:100 in 1% HNO_3. Rubidium was used as internal standard. ICP-MS measurements were performed to determine the corresponding concentration of dissolved zinc released by $ZnCl_2$ (Sigma-Aldrich, Switzerland). Here, strictly speaking, the dissolved Zn(II) species is not pure. The main dissolved species is $Zn^{2+}_{(aq)}$, followed by minor amounts of $ZnCl^{+}_{(aq)}$ and $Zn(OH)^{+}_{(aq)}$. The concentrations of soluble Zn(II) released by suspended nZnO at exposure concentrations of 0.2, 1 and 5 mg/L correspond to Zn(II) concentrations of 0.1, 0.5, and 2.2 mg/L, respectively.

At each sampling time point, 3 embryos of each of the 4 replicates were washed twice in 1 mM EDTA and individually dissolved in 300 µL aqua regia (3:1 HCl:HNO_3) for two days. If not hatched, additional 3 embryos per replicate were dechorionated, and chorion as well as dechorionated embryos dissolved in aqua regia separately. Samples were diluted 1:20 in HPLC-grade Nanopure water. Quality control measures included the use of procedural blanks.

2.3 Laser-ablation inductively-coupled-plasma mass-spectrometry (LA-ICP-MS) imaging

At each time point, embryos of the highest dose groups and controls were dehydrated and embedded in agarose according to the protocol of Sabaliauskas et al. (2006). A microtome (SM2010R, Leica) was used to prepare embryo cross sections with a flat surface. A NWR213 laser ablation system (ESI, Portland, USA) was coupled to the above ICP-MS system for bioimaging, yet without using helium as collision gas. This allowed the qualitative assessment of element distribution in zebrafish embryo cross sections. The laser was operated at 50% of its maximal energy (fluence of 6.8 J / cm ²), at 20 Hz firing rate, at an ablation rate of 25 µm / sec, and with a focussed spot size of 20 µm. Single lines (3.6 mm long) were recorded with a line spacing of 20 µm. All embryos of the same time point were run in the same analysis to ensure relative comparison. The measured isotope data of zinc (^{66}Zn for mapping; ^{64}Zn for verification of mapping results) and calcium (^{43}Ca) were exported and converted into images

using the Iolite software running on IGOR Pro 6 (WaveMetrics, USA). The development of a reliable quantification strategy would go beyond the scope of this study (Becker, 2013), yet the technique allowed the determination of the spatial element distribution and comparison of the relative intensities of exposed embryos and eleuthero-embryos to controls.

2.4 Experimental design

Zebrafish eggs were supplied by Harland Laboratories (Itingen, Switzerland). Fertilized eggs were washed twice with autoclaved Holtfreter's medium. Embryos in the blastula stage were selected for subsequent control and exposure experiments in covered glass beakers containing 250 mL of Holtfreter's medium (3.5 g NaCl, 0.2 g $NaHCO_3$, 0.05 g KCl, 0.12 g $CaCl_2$ and 0.1 g alginic acid per litre at pH 7). The supplementation of alginic acid leads to smaller and more stable nanoparticle aggregate sizes, as assessed in a previous pilot study (George et al. 2011). Stock solutions of nZnO and $ZnCl_2$ (both 1 mg/mL) were prepared in Nanopure water, stirred for 30 minutes and ultrasonicated for 5 minutes before dispersing in the media. To ensure homogenous nanoparticle dispersion, each beaker was aerated with a glass pipet. Throughout the experiments a 16 h light: 8 h dark photoperiod was used.

A static-renewal procedure was applied with complete water exchange every 24 h, by carefully transferring the embryos to new beakers containing medium and the appropriate concentrations of nZnO and $ZnCl_2$, respectively. Two exposure scenarios have been chosen. First, embryos were exposed from 0-96 hours post fertilization (hpf). The embryos were protected by the chorion. Second, newly hatched eleuthero-embryos were exposed from 72-168 hpf. Embryos and eleuthero-embryos were exposed for the same period of time to 0.2, 1, 5 mg/L nZnO, as well as to the corresponding concentrations of 0.27, 1.30, 5.74 mg/L $ZnCl_2$ given in Table 1. All of the three nZnO and $ZnCl_2$ concentrations have similar free zinc ion concentrations as determined by ICP-MS (0.1, 1 and 2.2 mg/L Zn(II)). Controls (media without nZnO or $ZnCl_2$) and each exposure concentration consisted of 240 embryos and eleuthero-embryos in total, respectively. Each dose-group consisted of four replicates

with 60 embryos each. For each exposure scenario, embryos and eleuthero-embryos, respectively, were sampled at two time points; 30 embryos from each of the 4 replicates were sampled at 48 and 96 hpf, 30 eleuthero-embryos from each of the 4 replicates at 120 and 168 hpf.

2.5 RNA isolation, reverse transcription, and quantitative real time RT-qPCR

Total RNA was isolated from pools of 25-30 zebrafish embryos using RNeasy Mini Kit (Qiagen, Basel, Switzerland). The RNA extraction procedure included a DNase I (Qiagen, Basel, Switzerland) treatment step to remove any contaminating genomic DNA. RNA concentrations and purity were measured spectrophotometrically using a NanoDrop ND-1000 Spectrophotometer (Nanodrop Technologies Inc. Wilsomington DE, U.S.). The RNA integrity was verified by visual inspection after agarose gel electrophoresis.

One microgram total RNA was reverse-transcribed using Moloney murine leukemia virus reverse transcriptase (Promega Bioscineces, Inc., Wallisellen, Switzerland) in the presence of random hexamers (Roche, Basel, Switzerland) and deoxynucleoside triphosphate (Sigma-Aldrich, Buchs, Switzerland). The reaction mixture was incubated for 5 min at 70°C, 1 h at 37°C, and the reaction was stopped by heating up to 95°C for 5 min.

Quantitative real-time PCR was performed with cDNAs and gene-specific primer pairs (Table 2) mixed with SYBR Green (FastStart Universal SYBR Green Master, Roche Diagnostics, Basel, Switzerland). The samples were denatured for 10 min at 95°C and then amplified using 40 cycles of 15 s at 95°C and 1 min at 58°C or 60°C (depending on transcript target), respectively, followed by quantitation using a melting curve analysis post run.

For calculating expression levels of selected genes, mRNA normalization was performed against the housekeeping gene (*RpL13α*), shown to be stable during the exposure period (Zucchi et al., 2012). The ΔC_T values were calibrated against the control ΔC_T values for all target genes. All reactions were run in duplicate using the BioRad CFX96 RealTime PCR Detection System (Biorad, Reinach, Switzerland). The amount of transcripts of selected target genes was expressed as fold

change (log2) according to the formula: 2^(ΔC_T untreated - ΔC_T treated).

2.6 Statistical analyses

The data were graphically illustrated with GraphPad Prism 5 (GraphPadSoftware, San Diega, Ca, U.S.). Significant differences between treatments were assessed by one way ANOVA followed by a Bonferroni posthoc test ($p \leq 0.05$) to compare treatment means of nanoparticulate exposure with Zn(II) exposure as well as treatment means with respective controls. Results are given as mean ± standard deviation of mean (SD). Differences were considered statistically significant at $p \leq 0.05$.

3. Results

3.1 Characterization of nZnO

The mean surface area of used nZnO was 68.7102 m^2/g, which is equivalent to a particle size of 9.4 nm (assuming a spherical shape), as determined under dry conditions by Brunauer-Emmet-Teller (BET) analysis (Table 1). Scanning electron microscopy (SEM) further confirmed the small size of the nZnO (Figure 1). However, considerable particle aggregation was observed, when measuring the size distribution of nZnO in the medium using nanoparticle tracking analysis (NTA). The larger hydrodynamic diameter, compared to BET, can be attributed to the tendency of particles to aggregate in the aqueous state.

Addition of alginic acid sodium salt (100 mg/L) to media resulted in a significantly reduced agglomeration size (Table 1). In Holtfreter's medium with alginate, the zeta potential was found to be -28.2 mV, in contrast to a potential around zero for media without such addition. The negatively charged natural acids will bind to the positively charged nanoparticles, which ultimately leads to a reduction in surface charge and to improved dispersion.

ICP-MS analysis was performed to quantify zinc ions released from nZnO and dissolved from $ZnCl_2$ in Holtfreter's media, respectively. For each of the nZnO concentration, the equivalent soluble Zn(II) concentration was prepared with appropriate concentrations of $ZnCl_2$. Dissolved Zn(II) concentrations were high upon contact with medium (average of 50.8% ± 3.7% of initial Zn) and stayed stable over 24 hours (52.7 ± 8.1% in average), demonstrating a rapid release of Zn(II) from nZnO. A fast dissolution reaching the equilibrium within 3 h (Xia et al. 2008) or 6 h (Mudunkotuwa et al. 2011) is already described and accounted for the presence of biological components and small particle size. The characteristics of used nZnO are summarized in Table 1.

3.2 Effect of nZnO and dissolved Zn(II) on hatching

At 72 hpf, hatching was significantly delayed in exposed embryos at all doses of nZnO and Zn(II)

compared to controls (Figure 2). At 96 hpf, almost all individuals (89.1 ± 12.7 % nZnO and 97.8 ± 2.6 % Zn(II)) of the lowest dose groups (0.2 mg/L nZnO and 0.27 Zn(II)) hatched, whereas only a few embryos (3.1 ± 2.7 % and 3.75 ± 3.1 % nZnO; 7.1 ± 9.4 % and 2 ± 2.7 % Zn(II) hatched in the mid and high dose groups (1 and 5 mg/L nZnO; 0.5, and 2.2 mg/L Zn(II)). No significant differences occurred between nZnO and corresponding Zn(II) concentrations. Therefore, we conclude the dissolution of Zn(II) from nZnO is the key determinant for the delayed and inhibited hatching.

3.3 Uptake of zinc into embryos and eleuthero-embryos

Embryos and eleuthero-embryos were exposed separately, and both were sampled after an exposure period of 48 and 96 h. The uptake of zinc by embryos, dechorionated embryos and chorion was compared. A dose-dependent increase in Zn content occurred in embryos and eleuthero-embryos (Figure 3). The content of Zn was also determined in the chorion, where a slightly increase in zinc was observed with exposure concentration at 48 and 96 hpf. Highest zinc accumulation occurred in embryos and eleuthero-embryos at the highest exposure concentrations. There was no significant difference in Zn(II) uptake between nZnO and $ZnCl_2$ exposures.

LA-ICP-MS profiles of embryos verified that Zn was accumulated and distributed across organs and tissues, rather than just adsorbed on the skin surface (Figure 4). At 48 hpf in nZnO exposed embryo and at 96 hpf, 120 hpf (48 h exposure) and 168 hpf (96 h exposure) in both nZnO and Zn(II) exposed embryos accumulation of Zn and its distribution in different tissues is clearly visible. Both nZnO and Zn(II) lead to comparably high Zn concentrations in the retina and pigment layers of the eyes, as well as in some parts of the brain, in the yolk sack and in the spinal cord. The cutting of the thin spinal cord was challenging and in some of the eleuthero-embryos even not possible. The distribution of ^{66}Zn (Figure 4) and of ^{64}Zn (Figure S1, supplementary material) were consistent, thus only ^{66}Zn is shown in Figure 4. In contrast to the Zn, Ca concentrations at 120 hpf and 168 hpf were decreased in the inner ear of exposed embryos as compared to controls.

3.4 Alteration of gene expression

Expressional changes of selected target genes were analysed after exposure to nZnO and Zn(II) for 48 h and 96 h in both embryos and eleuthero-embryos, respectively. In both stages, mRNA levels of genes related to oxidative stress including *cat* and *Cu/Zn-sod*, metallothionein (*mt2*), and immune responsive and pro-inflammatory genes (*TNFα, IL-1β, c-jun, Stat1a, MxA)* were determined by RT-qPCR. Expression of *cat* and *Cu/Zn-sod* showed a similar temporal pattern for both nZnO and Zn(II) with an up-regulation at 48 hpf in embryos and a down-regulation at 96 hpf at the highest concentrations (Figure 5). In eleuthero-embryo exposures *cat* and *Cu/Zn-sod* showed a down-regulation after 48 h of exposure at 120 hpf, whereas no alterations occurred at 168 hpf after 96 h of exposure (Figure 5). Transcripts of *mt2* were significantly up-regulated in embryos at 48 hpf and 96 hpf at almost all nZnO and Zn(II) concentrations, and at 5 mg/L nZnO and 2.2 mg/L Zn(II) in eleuthero-embryos at 120 and 168 hpf (Figure 5).

Transcripts of the pro-inflammatory cytokines, tumor necrosis factor-α (*TNFα*) and interleukin-1β (*IL-1β*), showed a different pattern in the embryo than eleuthero-embryo-exposures. A tendency for down-regulation of *TNFα* occurred in the embryo exposures (particularly at 96 hpf) after Zn(II) and nZnO treatment, while an induction occurred in eleuthero-embryo exposures at 120 hpf for both nZnO and Zn(II) (Figure 6). The expression pattern of *IL-1β* was similar, showing an up-regulation in eleuthero-embryo exposures, mainly after nZnO treatment. Additionally, the jun proto-oncogene (*c-jun*) was significantly up-regulated at 96 hpf in embryo exposures at mid and high doses of nZnO and Zn(II), but was not altered in eleuthero-embryo exposures (Figure 6). Both nZnO and Zn(II) exposures resulted in a significant down-regulation of the anti-viral and immune-related gene Myxovirus resistance A (*MxA*), while the signal transduction and activation of transcription 1a (*Stat1a*) remained unaffected (Figure 7).

Overall, the nZnO and Zn(II) induced expressional changes were more pronounced in embryo exposures than in eleuthero-embryo exposures. This suggests that embryos at an early stage, although protected by the chorion, react more sensitively to nZnO and Zn(II) than hatched eleuthero-embryos.

4. Discussion

The present study demonstrates dose-dependent effects of nZnO at individual size of 9.4 nm (BET), which tend to agglomerate in medium to a size of 196-242 nm (Nanosight, Table 1). Exposure of zebrafish embryos and eleuthero-embryos lead to an accumulation of zinc (Figure 3). Dose-dependent adverse effects on hatching (Figure 2) and expressional changes of genes associated with oxidative stress (Figure 5) and inflammation reaction (Figures 6, 7) occurred. Our data confirm previous reports on inhibitory effect of nZnO on hatching of embryos (Bai et al. 2010; Zhao et al. 2013), and they contribute to the understanding of the causes behind their effects. The effects were mainly related to the release of Zn(II) from nanoparticles, and they were more pronounced in embryos than eleuthero-embryos. There is still a debate on this question, as there are supporting reports (Song et al. 2010; Bürki-Turnherr 2013), as well as reports showing that zinc ions only partly contributed to the effects of nZnO (Bai et al. 2010; Ong et al. 2013; Zhao et al. 2013; Zhu et al. 2009).

Alginate added to the medium resulted in a stabilization of particles suspension, as indicated by NTA and Zeta potential measurements. Particles with a zeta potential greater than 30 mV, or lower than -30 mV, tend to repel each other, and are therefore considered to be a stable colloidal system (Webb and Orr, 1997). This indicates increased particle mobility under environmentally relevant conditions. Enhanced particle stability by dissolved natural organic matter (NOM), Suwannee River humic acid or biogenic molecules (proteins) is also found to crucially determine particle fate / transport for other nanoparticles (Chen et al., 2006; Hyung et al., 2007; Zhou and Keller, 2010; Omar et al., 2014). An increased negative surface charge of nanoparticles occurs in NOM-fortified medium, whereas a negative charge can be neutralized by adding counter cations (Zhang et al. 2009). Although Holtfreter's medium used in our study contains a rather high salt concentration, and therefore having a relatively high ionic strength, we could not observe the counteraction of the multivalent cations. The solubility of nZnO is highly dependent on the matrix in which they are suspended; a quicker and higher zinc dissolution occurs in complex cell culture media, or in presence of serum albumin compared with nanopure or moderately hard water (Reed et al., 2012). Furthermore, the presence of anions (e.g. Cl^-)

can serve as Zn^{2+} binding ligands, and thus accelerate nZnO dissolution. The small initial particle size of 9.4 nm might promote dissolution, considered to be proportional to the specific surface area of nanoparticles (Borm et al., 2006). Increasing solubility with decreasing nZnO size has been reported (Reed et al., 2012). In addition, the solubility of nZnO is highly pH-dependent. Over a pH range of 7 to 8, $Zn^{2+}_{(aq)}$ is the dominant species with $Zn(OH)^{+}_{(aq)}$ being present as well (Reichle et al., 1975).

The free metal ions are the bioavailable species and therefore mostly responsible for the here observed effects. Our study demonstrates that Zn(II) released from nZnO became accumulated in zebrafish embryos and eleuthero-embryos (Figures 3, 4). In the first 48 hours after fertilization, the chorion seems to protect the embryo by adsorption of nZnO and associated Zn(II) or blocking its transport through the pore canals. In contrast, after 96 hours an increased uptake of zinc was measured in embryos, indicating an uptake of nZnO and/or Zn(II). In such embryos, uptake and transport of Zn(II) is mediated by zinc-Iron related transporter proteins (ZIP) in the plasma membrane involved in the regulation of intracellular zinc level (Gaither and Eide, 2001). Possibly, binding sites on the chorion are fully occupied and zinc is starting to trespass the chorion after 48 hpf, and concomitant with the need for oxygen and minerals from the aquatic environment zinc was taken up. Although chorion pore canals are approximately 500-700 nm in diameter (Lee et al., 2009), agglomerates of nanoparticles of about 200 nm (as is the case for nZnO of this study, Table 1) can be already too large to be incorporated. This is based on the fact that not only the size but also the surface charge is a determining factor for uptake (Fent et al., 2010).

Our LA-ICP-MS analysis shows for the first time the uptake and embryonic tissue distribution pattern of zinc after exposure to nZnO and Zn(II) (Figure 4). Due to known interference of zinc divalent cations with calcium, both elements were monitored and compared. The distribution patterns of zinc and calcium were strikingly different. We suggest that higher uptake occurs due to the high demand of Zn, and possibly the higher activity and presence of uptake transporters in these tissues. Zinc is accumulated prominently in the retina and pigment layer of the eyes, in brain structures spinal cord and yolk sac, whereas in these tissues, calcium showed no increase (compare spots 1-5; Figure 4). In contrast, calcium was decreased in the inner ear. In zebrafish embryos uptake of gas and nutrients

occurs mainly through the body surface. Skin chloride cells were suggested to be the main site for Ca^{2+} influx before the complete development of the gills (Van der Heijden et al., 1999). Chloride cells start to differentiate in the skin of embryos at 48 hpf and active transport of Ca^{2+} is suggested (Hwang et al., 1994). It is likely that zinc is competitive with calcium and therefore impairing its uptake. As the process is in the skin of embryos, a large surface is affected. Hence, embryos show strong zinc uptake with calcium depletion. The reason for the specific calcium loss in the inner ear remains to be investigated. Similar as in zebrafish in our study, cellular uptake of Zn(II) caused a net loss of Ca^{2+} in brown trout fry (Sayer et al., 1991) and adult mud minnows (Sauer and Watabe, 1988).

Induction of ROS upon nZnO exposure has been reported in zebrafish embryos (Zhu et al. 2009; Zhao et al. 2013), activating or inhibiting several antioxidant enzymes. As a consequence, this may result in oxidative damage in zebrafish early life stages. To mitigate adverse effects of ROS, superoxide anions are converted to H_2O_2 by SOD, and O_2 by CAT (Valavanidis et al., 2006). In our study, exposure to nZnO and Zn(II) lead to up-regulation of both *Cu/Zn sod* and *cat* at 48 hpf, indicating a reaction to elevated ROS levels and thus, an induction of oxidative stress at 48 hpf. At 96 hpf, in contrast, *Cu/Zn sod* and *cat* were down-regulated, which may be related to a potential negative feedback mechanism at this time point in embryos. In eleuthero-embryos the down-regulation of *cat* and *Cu/Zn sod* at 120 hpf indicates an imbalance of Zn(II)-induced ROS. An increased SOD but decreased CAT enzyme activity was reported in zebrafish embryos (144 hpf) exposed to nZnO (Zhao et al. 2013). This suggests that the expressional pattern of these genes (and ROS levels) is not only related to Zn(II) concentrations, but also to the exposure time and time of sampling. The expression pattern induced by nZnO and Zn(II) was time-dependent and changed at different developments stages. Similar to our study, effects of nZnO in a human cell line were mainly based on the uptake of released Zn(II), followed by apoptosis (Bürki-Turnherr 2013).

In contrast to *cat* and *Cu/Zn sod*, transcripts of *mt2* were significantly increased at all exposure times in embryos and eleuthero-embryos. Up-regulation is governed by free Zn(II) and persisted during exposure to nZnO and Zn(II) to protect against high Zn(II) concentrations and oxidative stress.

Both *TNFα* and *IL-1β* play a critical role in initiating the pro-inflammatory cytokine cascade,

apoptosis, cell differentiation, and in stimulation of the adaptive immune response (Grayfer and Belosevic, 2012). Oxidative stress can activate pro-inflammatory signalling pathways (Xia et al., 2008). In human cell lines nZnO can lead to acute cytokine and chemokine generation, inducing inflammation (Kermanizadeh et al., 2012; Feltis et al., 2012). Moreover, ZnO nanoparticles and fine particles provoke similar inflammation on the rat lung exposed by inhalation (Warheit et al., 2009).

Here, we describe for the first time a down-regulation of *TNFα* and *IL-1β* in zebrafish embryos exposed to nZnO and Zn(II), and a significant up-regulation in eleuthero-embryos (Figure 6), which indicates a stimulation of the inflammatory immune response. Additionally, the *c-jun* proto-oncogene, which is a member of the *c-Jun* N-terminal protein kinase (JNK) signalling pathway, was significantly up-regulated. The activation of redox-sensitive JNK and pro-inflammatory cytokines, such as *TNFα* and *IL-1β*, lead to induction of genes for cytokines, chemokines and various pro-inflammatory mediators, which play an important role in the inflammatory response (Ip and Davis, 1998). We therefore conclude that exposure to nZnO and Zn(II) leads to modulation of pro-inflammatory responses in embryos and eleuthero-embryos.

5. Conclusion

Our present study sheds new lights on the potential effects of nZnO in zebrafish early life stages. To determine whether effects of nZnO are based on the free Zn(II) concentration, we exposed early life stages of zebrafish to nZnO and to equal concentrations of released free Zn(II) derived from $ZnCl_2$. Both nZnO and $ZnCl_2$ showed a similar hatching interference, uptake and distribution in embryos and eleuthero-embryos, and they induced similar dose-related effects on gene expression. This leads to the conclusion that the biological activity of nZnO is mainly based on the released free Zn(II) concentration. The nanoparticle nature itself contributed very little to the effects, therefore we conclude that the nanoparticulates themselfs are not taken up. This is further evidenced by bioimaging. Figure 4 showed

no evident spots of zinc, which would originate from nanoparticle accumulation. As images of nZnO and Zn(II) are similar, we conclude that Zn(II) but not nZnO do enter the embryo.

The current study adds to the existing data by exploring a series of different target molecular pathways. Novel are potential pro-inflammatory effects of nZnO and Zn(II), indicated by the up-regulation of *TNFα* and *IL-1β* in eleuthero-embryos. More pronounced expressional changes indicated higher sensitivity of embryo exposures in contrast to eleuthero-embryo exposures. Thus, embryos reacted more sensitively to nZnO and Zn(II) although potentially protected by the chorion. Reasons for the higher sensitivity are unknown but also found with other environmental pollutants (Zucchi et al. 2012). Thus, nZnO agglomerates adsorbed to the chorion are indicated to release Zn(II), which are responsible for the observed effects. The most prominent expressional changes were the induction of *mt2* and alterations in the oxidative stress related genes *sod* and *cat*. Alteration of pro-inflammatory genes *TNFα* and *IL-1β* implies that nZnO and Zn(II) result in modulation of pro-inflammatory reactions. Estimated concentrations of nZnO are expected in the range of 0.3-0.4 µg/L in sewage treatment plant effluents (Nowack and Bucheli, 2007). Despite nZnO concentrations used in our present study are much higher, our data contribute to the understanding of the potential hazards and effects of nZnO in the aquatic environment.

Declaration of interest

The authors report no conflicts of interest.

Acknowledgements

We thank Erik Ammann, FHNW, for SEM pictures and Genes'Ink (Marseille, France) for providing nZnO. This study was supported by the European Commission (contract EC-FP7-SUNFLOWER-287594).

References

Bai W, Zhang Z, Tian W, He X, Ma Y, Zhao Y, Chai Z. Toxicity of zinc oxide nanoparticles to zebrafish embryo: a physicochemical study of toxicity mechanism. J Nanopart Res 2009;12:1645–1654.

Becker SJ. Imaging of metals in biological tissue by laser ablation inductively coupled plasma mass spectrometry (LA-ICP-MS): state of the art and future developments. J Mass Spectrom 2013;48:255–268.

Bian SW, Mudunkotuwa IA, Rupasinghe T, Grassian VH. Aggregation and dissolution of 4 nm ZnO nanoparticles in aqueous environments: influence of pH, ionic strength, size, and adsorption of humic acid. Langmuir 2011;27:6059–6068.

Blinova I, Ivask A, Heinlaan M, Mortimer M, Kahru A. Ecotoxicity of nanoparticles of CuO and ZnO in natural water. Environ Pollut 2010;158:41–47.

Borm P, Klaessig FC, Landry TD, Moudgil B, Pauluhn J, Thomas K, Trottier R, Wood S. Research strategies for safety evaluation of nanomaterials, part V: role of dissolution in biological fate and effects of nanoscale particles. Toxicol Sci 2006;90:23–32.

Brunauer S, Emmet PH, Teller E. Adsorption of gases in multimolecular layers. J Am Chem Soc 1938;60:309–319.

Buerki-Thurnherr T, Xiao L, Diener L, Arslan O, Hirsch C, Maeder-althaus X, Grieder K, Wampfler B, Mathur S, Wick P, Krug H. In vitro mechanistic study towards a better understanding of ZnO nanoparticle toxicity. Nanotoxicology 2013;7:402–416.

Buffle J, Altmann RS, Filella M, Tessier A. Complexation by natural heterogeneous compounds: Site occupation distribution functions, a normalized description of metal complexation. Geochim Cosmochim Ac. 1990;54:1535–1553.

Chen KL, Mylon SE, Elimelech M. Aggregation Kinetics of Nanoparticles in Monovalent and Divalent Electrolytes. Environ Sci Technol. 2006;40:1516–1523.

Degen A, Kosec M. Effect of pH and impurities on the surface charge of zinc oxide in aqueous solution. J Eur Ceram Soc. 2000;20:667–673.

Dineley KE, Votyakova TV, Reynolds IJ. Zinc inhibition of cellular energy production: implications for mitochondria and neurodegeneration. J Neurochem. 2003;85:563–570.

Feltis BN, Okeefe SJ, Harford AJ, Piva TJ, Turney TW, Wright PFA. Independent cytotoxic and inflammatory responses to zinc oxide nanoparticles in human monocytes and macrophages. Nanotoxicology. 2012;6:757–765.

Fent K, Weisbrod CJ, Wirth-Heller A, Pieles U. Assessment of uptake and toxicity of fluorescent silica nanoparticles in zebrafish (*Danio rerio*) early life stages. Aquat Toxicol. 2010;100:218–228.

Fernández D, García-Gómez C, Babín M. In vitro evaluation of cellular responses induced by ZnO nanoparticles, zinc ions and bulk ZnO in fish cells. Sci Total Environ. 2013;452-453:262–274.

Franklin NM, Rogers NJ, Apte SC, Batley GE, Gadd GE, Casey PS. Comparative Toxicity of Nanoparticulate ZnO, Bulk ZnO, and $ZnCl_2$ to a Freshwater Microalga (*Pseudokirchneriella subcapitata*): The Importance of Particle Solubility. Environ Sci Technol. 2007;41:8484–8490.

Gaither LA, Eide DJ. The human ZIP1 transporter mediates zinc uptake in human K562 erythroleukemia cells. J Biol Chem. 2001;276:22258–22264.

George S, Lin S, Ji Z, Thomas CR, Li L, Mecklenburg M, Meng H, Wang X, Zhang H, Xia T, Hohman JN, Lin S, Zink JI, Weiss PS, Nel AE. Surface defects on plate-shaped silver nanoparticles contribute to its hazard potential in a fish gill cell line and zebrafish embryos. ACS Nano. 2012;6:3745–3759.

George S, Xia T, Rallo R, Zhao Y, Ji Z, Lin S, Wang X, Zhang H, France B, Schoenfeld D, Damoiseaux R, Liu R, Lin S, Bradley KA, Cohen Y, Nel AE. Use of a high-throughput screening approach coupled with in vivo zebrafish embryo screening to develop hazard ranking for engineered nanomaterials. ACS Nano. 2011;5:1805–1817.

Grayfer L, Belosevic M. Cytokine regulation of teleost inflammatory responses. In: Türker H. (Eds.), New Advances and Contributions to Fish Biology. Published by InTech, Croatia. 2012;pp. 59–96.

Handy RD, Owen R, Valsami-Jones E. The ecotoxicology of nanoparticles and nanomaterials: current status, knowledge gaps, challenges, and future needs. Ecotoxicology. 2008;17:315-325.

Hanley C, Thurber A, Hanna C, Punnoose A, Zhang J, Wingett DG. The Influences of cell type and ZnO nanoparticle size on immune cell cytotoxicity and cytokine induction. Nanoscale Res Lett. 2009;4:1409–1420.

Heng BC, Zhao X, Xiong S, Ng KW, Boey FYC, Loo JSC. Toxicity of zinc oxide (ZnO) nanoparticles on human bronchial epithelial cells (BEAS-2B) is accentuated by oxidative stress. Food Chem Toxicol. 2010;48:1762–1766.

Hu X, Cook S, Wang P, Hwang HM. In vitro evaluation of cytotoxicity of engineered metal oxide nanoparticles. Sci Total Environ. 2009;407:3070–3072.

Hwang P, Tsail Y, Tung Y. Calcium balance in embryos and larvae of the freshwater-adapted teleost, Oreochromis mossambicus. Fish Physiol Biochem. 1994;13:325–333.

Hyung H, Fortner JD, Hughes JB, Kim JH. Natural organic matter stabilizes carbon nanotubes in the aqueous phase. Environ Sci Technol. 2007;41:179–184.

Ip TY, Davis RJ. Signal transduction by the c-Jun N-terminal kinase (JNK) - from inflammation to development. Curr Opin Cell Biol. 1998;10:205–219.

Kermanizadeh A, Pojana G, Gaiser BK, Birkedal R, Bilaničová D, Wallin H, Jensen KA, Sellergren B, Hutchison GR, Marcomini A, Stone V. In vitro assessment of engineered nanomaterials using a hepatocyte cell line: cytotoxicity, pro-inflammatory cytokines and functional markers. Nanotoxicology. 2013;7:301–313.

Lee KJ, Nallathamby PD, Browning LM, Christopher J, Xu XN. In Vivo imaging of transport and biocompatibility of single silver nanoparticles in early development of zebrafish embryos. ACS Nano. 2009;1:133–143.

Li S, Wallis LK, Ma H, Diamond SA. Phototoxicity of TiO2 nanoparticles to a freshwater benthic amphipod: Are benthic systems at risk? Sci Total Environ. 2014; 466-467:800-808.

Li S, Canas-Carrell JE, Irin F, Atore FO, Green MJ. Determination of multi-walled carbon nanotube bioaccumulation in earthworms measured by a microwave-based detection technique. Sci Total Environ. 2013; 445-446:9-13.

Mudunkotuwa IA, Rupasinghe T, Wu CM, Grassian VH. Dissolution of ZnO nanoparticles at circumneutral pH: a study of size effects in the presence and absence of citric acid. Langmuir. 2011;28:396–403.

Nel A, Xia T, Mädler L, Li N. Toxic potential of materials at the nanolevel. Science. 2006;311:622–627.

Nowack B, Bucheli TD. Occurrence, behavior and effects of nanoparticles in the environment. Environ Pollut. 2007;150:5–22.

Omar MF, Aziz HA, Stoll S. Aggregation and disaggregation of ZnO nanoparticles: Influence of pH and adsorption of Suwannee River humic acid. Sci Total Environ. 2014;468-469:195–201.

Ong K, Zhao X, Thistle M, Maccormack TJ, Clark RJ, Ma G, Martinez-Rubi Y, Simard B, Loo J, Veinot JG, Goss GG. Mechanistic insights into the effect of nanoparticles on zebrafish hatch. Nanotoxicology. 2013;8:295-304.

Poynton HC, Lazorchak JM, Impellitteri CA, Smith ME, Rogers K, Patra M, Hammer KA, Allen HJ, Vulpe CD. Differential gene expression in Daphnia magna suggests distinct modes of action and bioavailability for ZnO nanoparticles and Zn ions. Environ Sci Technol. 2011;45:762–768.

Reed RB, Ladner DA, Higgins CP, Westerhoff P, Ranville JF. Solubility of nano-zinc oxide in environmentally and biologically important matrices. Environ Toxicol Chem. 2012;31:93–99.

Reichle RA, McCurdy KG, Hepler LG. Zinc hydroxide: solubility product and hydroxy-complex stability constants from 12.5-75 °C. Can J Chem. 1975;53:3841–3845.

Sabaliauskas NA, Foutz CA, Mest JR, Budgeon LR, Sidor AT, Gershenson JA, Joshi SB, Cheng KC. High-throughput zebrafish histology. Methods. 2006;39:246–254.

Sauer GR and Watabe N. The effects of heavy metals and metabolic inhibitors on calcium uptake by gills and scales of *Fundulus hetroclitus in vitro*. Comp Biochem Physiol. 1988;91C:473-478.

Sayer MD, Reader JP, Morris R. Effects of six trace metals on calcium fluxes in brown trout (*Salmo trutta L.*) in soft water. J Comp Physiol. 1991;161:537–542.

Sensi SL, Yin HZ, Carriedo SG, Rao SS, Weiss JH. Preferential Zn^{2+} influx through Ca^{2+}-permeable AMPA/kainate channels triggers prolonged mitochondrial superoxide production. PNAS. 1999;96:2414–2419.

Sharma V, Anderson D, Dhawan A. Zinc oxide nanoparticles induce oxidative DNA damage and ROS-triggered mitochondria mediated apoptosis in human liver cells (HepG2). Apoptosis. 2012;17:852-870

Shaw BJ, Handy RD. Physiological effects of nanoparticles on fish: a comparison of nanometals versus metal ions. Environ Int. 2011;37:1083–1097.

Song W, Zhang J, Guo J, Zhang J, Ding F, Li L, Sun Z. Role of the dissolved zinc ion and reactive oxygen species in cytotoxicity of ZnO nanoparticles. Toxicol Lett. 2010;199:389–397.

Valavanidis A, Vlahogianni T, Dassenakis M, Scoullos M. Molecular biomarkers of oxidative stress in aquatic organisms in relation to toxic environmental pollutants. Ecotox Environ Safe. 2006;64:178–189.

Van der Heijden A, Van der Meij J, Flik G, Wendelaar Bonga S. Ultrastructure and distribution dynamics of chloride cells in tilapia larvae in fresh water and sea water. Cell Tissue Res. 1999.;297:119–130.

Warheit DB, Sayes CM, Reed KL. Nanoscale and fine zinc oxide particles: can in vitro assays accurately forecast lung hazards following inhalation exposures? Environ Sci Technol. 2009;43:7939–7945.

Webb PA, Orr C. Analytical Methods in Fine Particle Technology. Micromeritics Instrument Corporation. 1997.

Wilkinson KJ, Balnois E, Leppard GG, Buffle J. Characteristic features of the major components of freshwater colloidal organic matter revealed by transmission electron and atomic force microscopy. Colloids Surf A. 1999;155:287–310.

Xia T, Kovochich M, Liong M, Mädler L, Gilbert B, Shi H, Yeh JI, Zink JI, Nel AE. Comparison of the mechanism of toxicity of zinc oxide and cerium oxide nanoparticles based on dissolution and oxidative stress properties. ACS Nano. 2008;2:2121–2134.

Xia T, Zhao Y, Sager T, George S, Pokhrel S, Li N, Schoenfeld D, Meng H, Lin S, Wang X, Wang M, Ji Z, Zink JI, Mädler L, Castranova V, Lin S, Nel AE. Decreased dissolution of ZnO by iron doping

yields nanoparticles with reduced toxicity in the rodent lung and zebrafish embryos. ACS Nano. 2011;5:1223–1235.

Zhang Y, Chen Y, Westerhoff P, Crittenden J. Impact of natural organic matter and divalent cations on the stability of aqueous nanoparticles. Water Res. 2009;43:4249–4257.

Zhao X, Wang S, Wu Y, You H, Lv L. Acute ZnO nanoparticles exposure induces developmental toxicity, oxidative stress and DNA damage in embryo-larval zebrafish. Aquat Toxicol. 136-2013;137:49–59.

Zhou D, Keller AA. Role of morphology in the aggregation kinetics of ZnO nanoparticles. Water Res. 2010;44:2948–2956.

Zhu X, Wang J, Zhang X, Chang Y, Chen Y. The impact of ZnO nanoparticle aggregates on the embryonic development of zebrafish (*Danio rerio*). Nanotechnology. 2009;20:1-9.

Zimmermann YS, Schäffer A, Hugi C, Fent K, Corvini PFX, Lenz M. Organic photovoltaics: Potential fate and effects in the environment. Environ Int. 2012;49.128-140.

Zucchi S, Castiglioni S, Fent K. Progestins and antiprogestins affect gene expression in early development in zebrafish (*Danio rerio*) at environmental concentrations. Environ Sci Technol. 2012;46:5183–92.

Tables

Table 1. Characteristics of nZnO.

Surface area (BET)	68.71 m^2/g	
Zeta potential ζ^1		
	0 h	**24 h**
Holtfreter's medium without Alginate	2.3 mV	- [2]
Holtfreter's medium with Alginate	- 27.2 mV	- 28.2 mV
Average Agglomeration Size (NTA)		
	0 h	**24 h**
5 mg/L without Alginate	218 ± 36 nm	336 ± 38 nm
0.2 mg/L with Alginate	196 ± 13 nm	211 ± 23 nm
1 mg/L with Alginate	214 ± 23 nm	236 ± 19 nm
5 mg/L with Alginate	223 ± 12 nm	242 ± 17 nm
Zn(II) release (ICP-MS)		
	0 h	**24 h**
nZnO low (0.2 mg/L)	0.106 ± 0.014 mg/L	0.116 ± 0.018 mg/L
$ZnCl_2$ low (0.27 mg/L)	0.092 ± 0.010 mg/L	0.097 ± 0.013 mg/L
nZnO mid (1 mg/L)	0.530 ± 0.061 mg/L	0.567 ± 0.098 mg/L
$ZnCl_2$ mid (1.30 mg/L)	0.508 ± 0.055 mg/L	0.501 ± 0.070 mg/L
nZnO high (5 mg/L)	2.327 ± 0.245 mg/L	2.169 ± 0.172 mg/L
$ZnCl_2$ high (5.75 mg/L)	2.249 ± 0.122 mg/L	2.192 ± 0.206 mg/L

[1] measured at pH 7 and 25 °C

[2] not measureable, particle precipitations clearly visible

Table 1. Primer Sequences for Quantitative Real-Time PCR Analysis.

Target gene	Primer Sequence (5' to 3')	Accession no.[a]
RpL13α	Forward: AGC TCA AGA TGG CAA CAC AG	NM_198143
	Reverse: AAG TTC TTC TCG TCC TCC	
Cat	Forward: AGG GCA ACT GGG ATC TTA CA	NM_130912
	Reverse: TTT ATG GGA CCA GAC CTT GG	
Cu/Zn-SOD	Forward: GGC CAA CCG ATA GTG TTA GA	NM_131294
	Reverse: CCA GCG TTG CCA GTT TTT AG	
MT2	Forward: AAA TGG ACC CCT GCG AAT	NM_001131053
	Reverse: TTG CAG GTA GCA CCA CAG TT	
TNFα	Forward: ACC AGG CCT TTT CTT CAG GT	NM_212859
	Reverse: TGC CCA GTC TGT CTC CTT CT	
IL-1β	Forward: CAT TTG CAG GCC GTC ACA	NM_212844
	Reverse: GGA CAT GCT GAA GCG CAC TT	
c-jun	Forward: ACG TGG GAC TTC TCA AAC TG	NM_199987
	Reverse: TCT TGG GAC ACA GAA ACT GG	
MxA	Forward: GAT CCC AAT GGT GAT CCG CTA C	NM_182942
	Reverse: TCA CAG TCC TCT TTA AGC AGG TTG TC	
Stat1a	Forward: TCA AAG GAG GAC CTG AAC CGC	NM_131480
	Reverse: CAA CAC CTC GGA CAT CTG ACT AAT C	

[a] GeneBank accession number (http://www.ncbi.nlm.nih.gov).

Figure Legends:

Figure 1. Scanning electron microscopic (SEM) image of ZnO nanoparticles. Scale bar 100 nm.

Figure 2. Cumulative percentage of hatched zebrafish embryos exposed different concentrations of nZnO and Zn(II). The hatching rate significantly decreased with increasing doses of nZnO and Zn(II); low refers to 0.1, mid to 0.5 and high to 2.2 mg/L dissolved zinc in exposure group with nanoparticulate ZnO (nZnO) and without (Zn(II)). Average value was calculated for a total of 120 embryos from four replicates with 30 embryos in each. Error bars represent standard deviation (SD). All exposed embryos at 72 hpf, and mid and high dose groups at 96 hpf show significant differences ($p < 0.05$) compared to control group.

Figure 3. Total Zn content in zebrafish embryos (48 and 96 hpf), dechorionated embryos and chorions in µg per embryo, as well as in eleuthero-embryos (120 and 168 hpf). Both nZnO and Zn(II) exposures result in a similar dose-related uptake of ^{66}Zn into embryos and eleuthero-embryos. Low refers to 0.1, mid to 0.5 and high to 2.2 mg/L dissolved zinc in exposure group with nanoparticulate ZnO (nZnO) and without (Zn(II)). At 96 hpf embryos of control and 0.1 mg/L (low dose group) were hatched. Asterisks indicate significant differences of dechorionated embryos to hatched controls (*$p < 0.05$, **$p < 0.01$, and ***$p < 0.001$). Error bars are + standard deviation (SD) of measured values for each exposure group consisting of 4 replicates (per replicate 3 embryos measured).

Figure 4. Pictures showing the embedded dechorionated embryos and eleuthero-embryos before LA-ICP-MS analysis (left) and Zn and Ca organ distribution measured by LA-ICP-MS (center and right). In each picture coronal zebrafish embryo sections of controls (embryo on the left), nZnO high (center) and Zn(II) high (right) exposure groups at different time points (48 hpf, 96 hpf, 120 hpf, 168 hpf) and exposure times (48 and 96 h, respectively) are shown. Spots of accumulation are labelled as (1) retina and pigment layers of the eyes, (2) brain, (3) yolk sack, (4) spinal cord, (5) inner ear. Colour bars show

the intensity in counts per seconds.

Figure 5. Transcriptional alterations of oxidative stress related genes catalase (*cat)*, Cu/Zn superoxide dismutase (*Cu/Zn sod*) and metallothionein (*mt2*) in zebrafish embryos (at 48 and 96 hpf or 48 and 96 h exposure, left) and eleuthero-embryos (at 120 and 168 hpf or 48 and 96 h exposure, right), respectively, exposed to 0.1, 0.5 and 2.2 mg/L of dissolved zinc in exposure groups with nanoparticulate ZnO (nZnO) and without (Zn(II)). Asterisks indicate significant differences to controls (*$p < 0.05$, **$p < 0.01$, and ***$p < 0.001$). Values are presented as mean ± SD (n=4).

Figure 6. Transcriptional alteration of innate immune system related genes *TNFα*, *IL-1β* and of *c-jun* in zebrafish embryos (at 48 and 96 hpf or 48 and 96 h exposure, left) and eleuthero-embryos (at 120 and 168 hpf or 48 and 96 h exposure, right), respectively, exposed to 0.1, 0.5 and 2.2 mg/L of dissolved zinc in exposure groups with nanoparticulate ZnO (nZnO) and without (Zn(II)). Asterisks indicate significant differences to controls (*$p < 0.05$, **$p < 0.01$, and ***$p < 0.001$). Values are presented as a mean ± SD (n=4).

Figure 7. Transcriptional alteration of interferon- and virus-inducible genes including *stat1a* and *MxA* in zebrafish embryos (at 48 and 96 hpf or 48 and 96 h exposure, left) and eleuthero-embryos (at 120 and 168 hpf or 48 and 96 h exposure, right), respectively, exposed to 0.1, 0.5 and 2.2 mg/L of dissolved zinc in exposure groups with nanoparticulate ZnO (nZnO) and without (Zn(II)). Asterisks indicate significant differences to controls (*$p < 0.05$, **$p < 0.01$, and ***$p < 0.001$). Values are presented as a mean ± SD (n=4).

Figure 1.

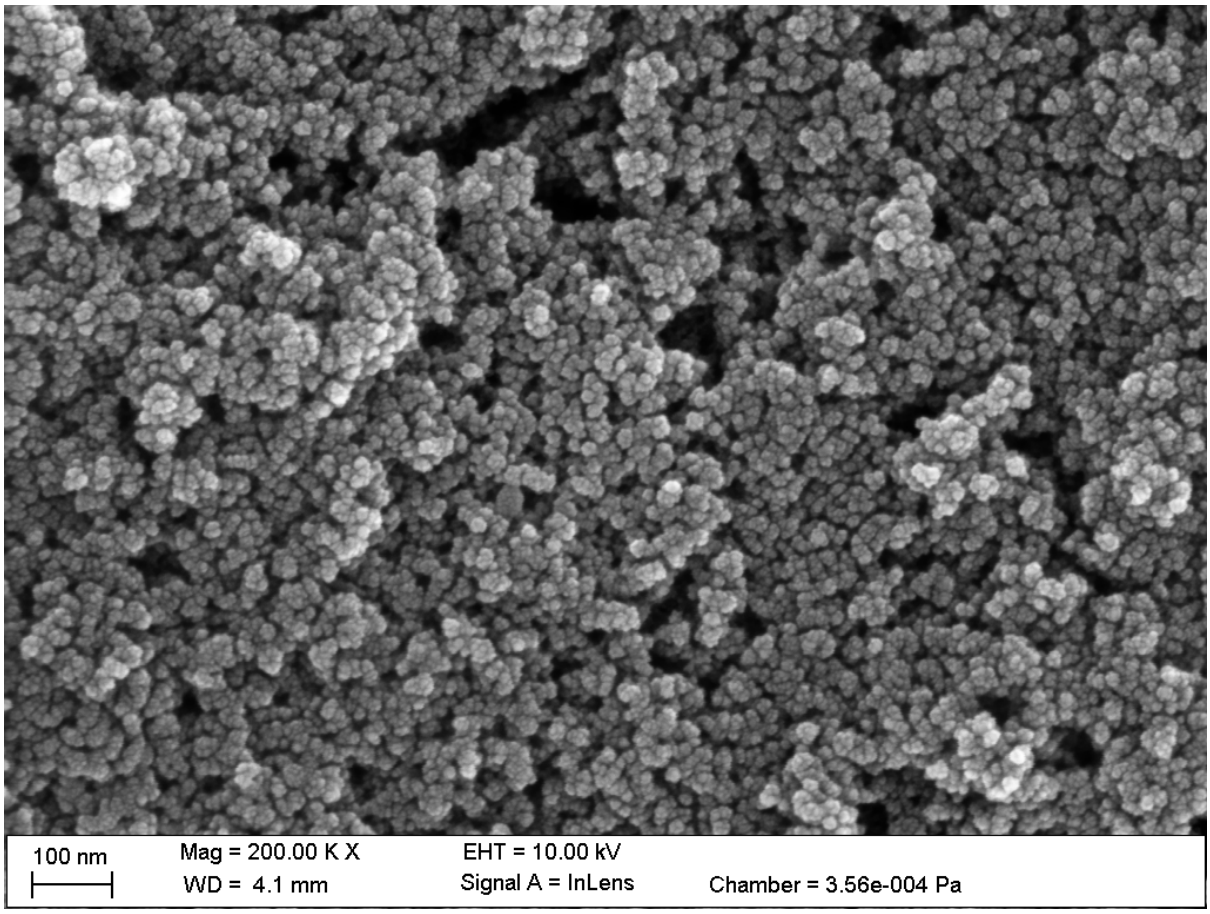

Figure 2.

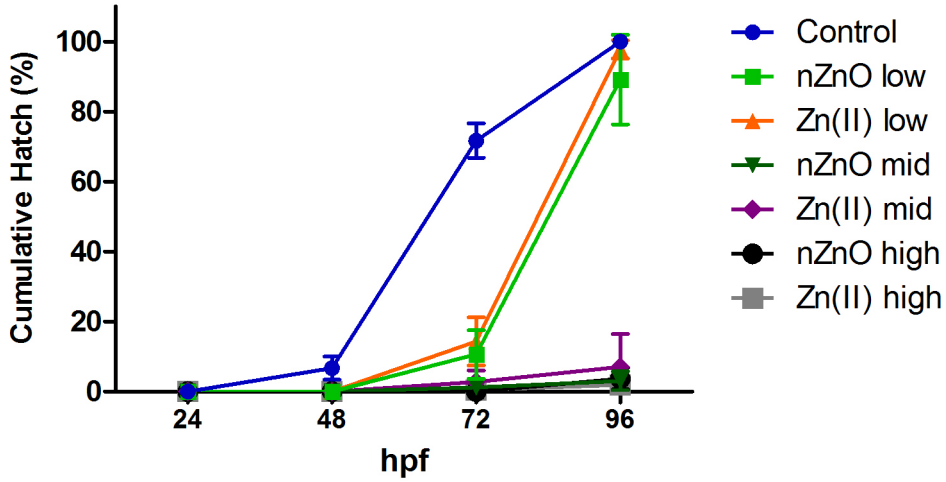

Figure 3

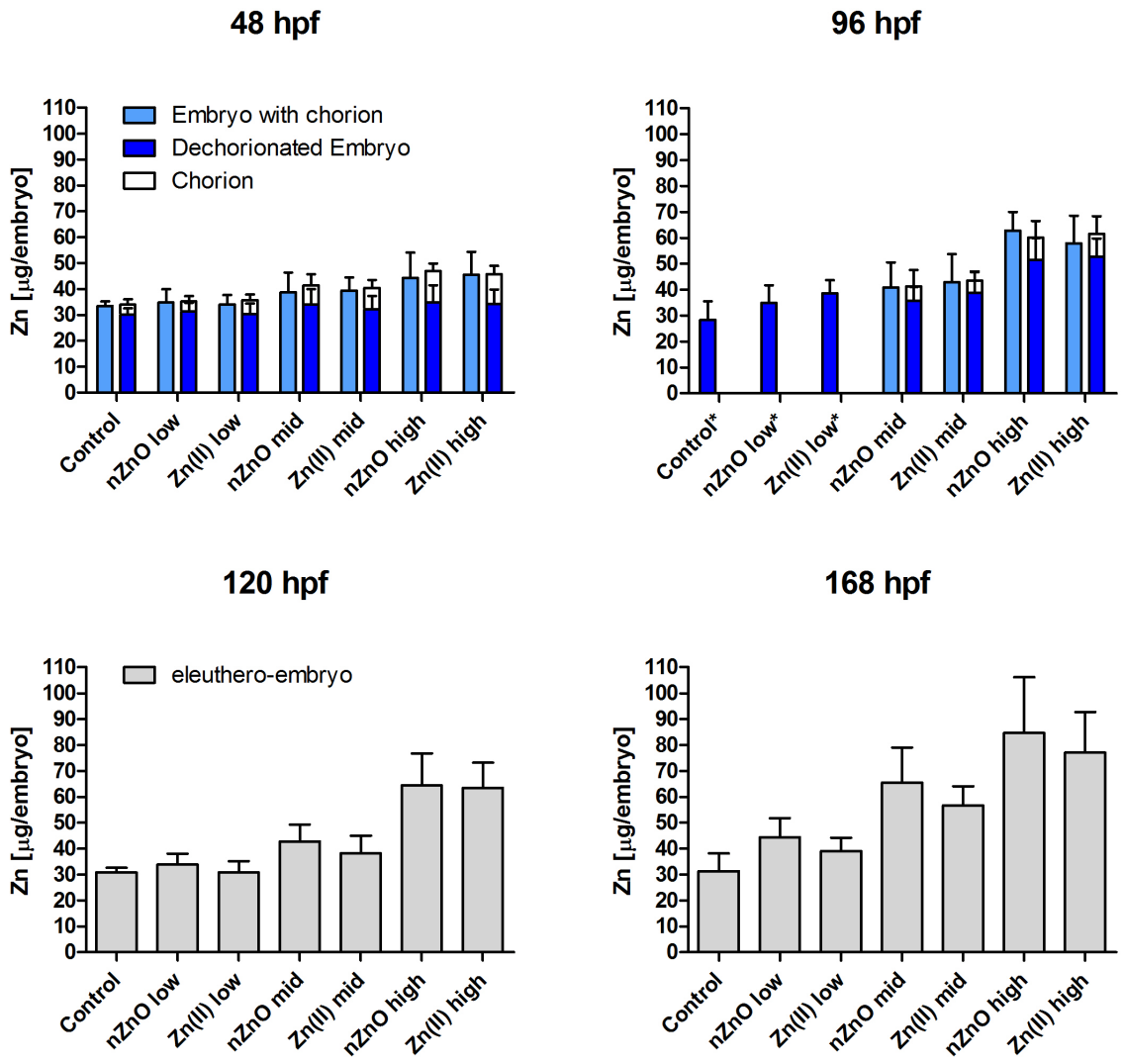
48 hpf
96 hpf
120 hpf
168 hpf
Embryo with chorion
Dechorionated Embryo
Chorion
eleuthero-embryo
Zn [µg/embryo]
Control
nZnO low
Zn(II) low
nZnO mid
Zn(II) mid
nZnO high
Zn(II) high
Control*
nZnO low*
Zn(II) low*

Figure 4

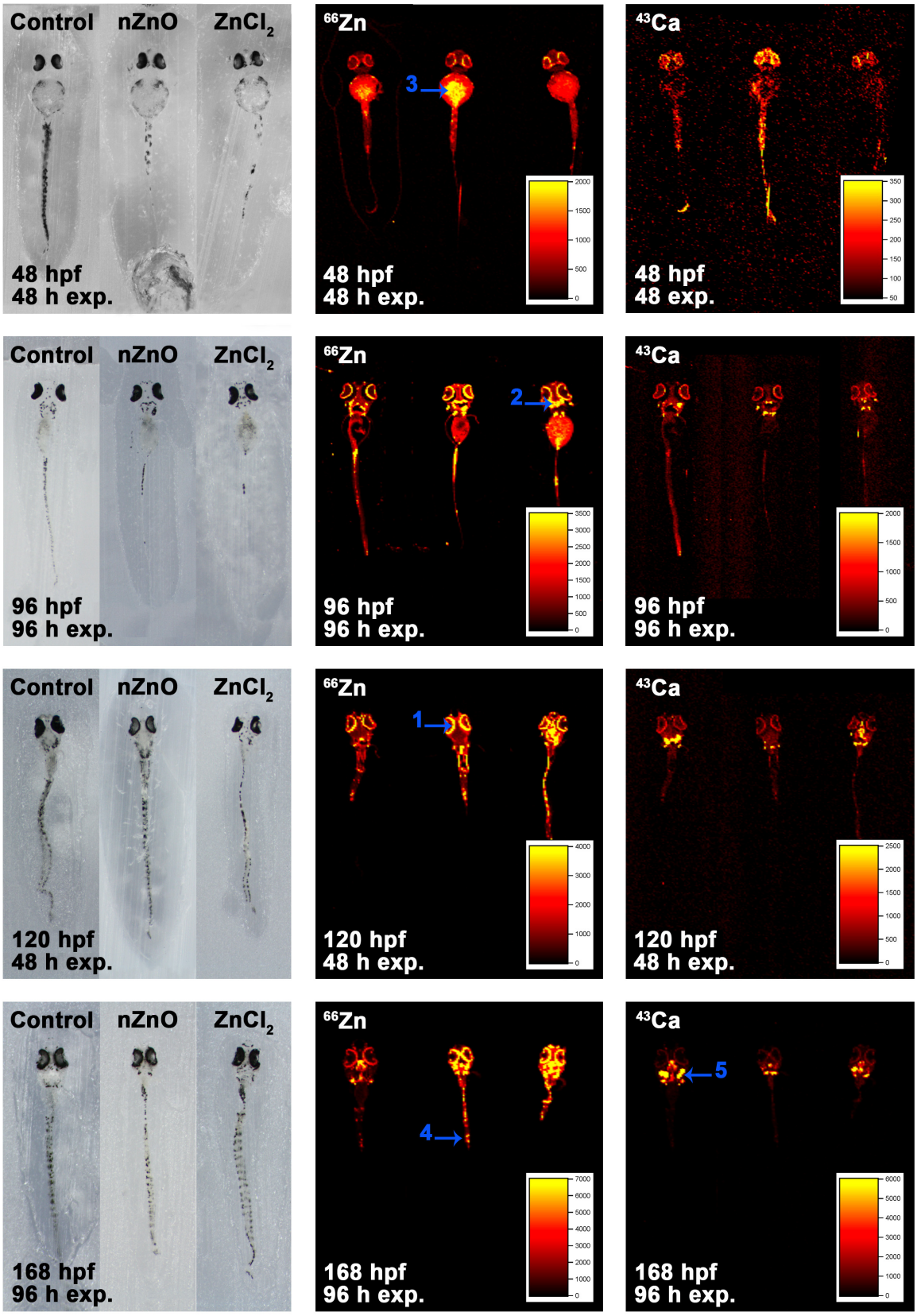
Control
nZnO
ZnCl2
48 hpf
48 h exp.
66Zn
3
48 hpf
48 h exp.
43Ca
48 hpf
48 exp.
Control
nZnO
ZnCl2
96 hpf
96 h exp.
66Zn
2
96 hpf
96 h exp.
43Ca
96 hpf
96 h exp.
Control
nZnO
ZnCl2
120 hpf
48 h exp.
66Zn
1
120 hpf
48 h exp.
43Ca
120 hpf
48 h exp.
Control
nZnO
ZnCl2
168 hpf
96 h exp.
66Zn
4
168 hpf
96 h exp.
43Ca
5
168 hpf
96 h exp.

Figure 5

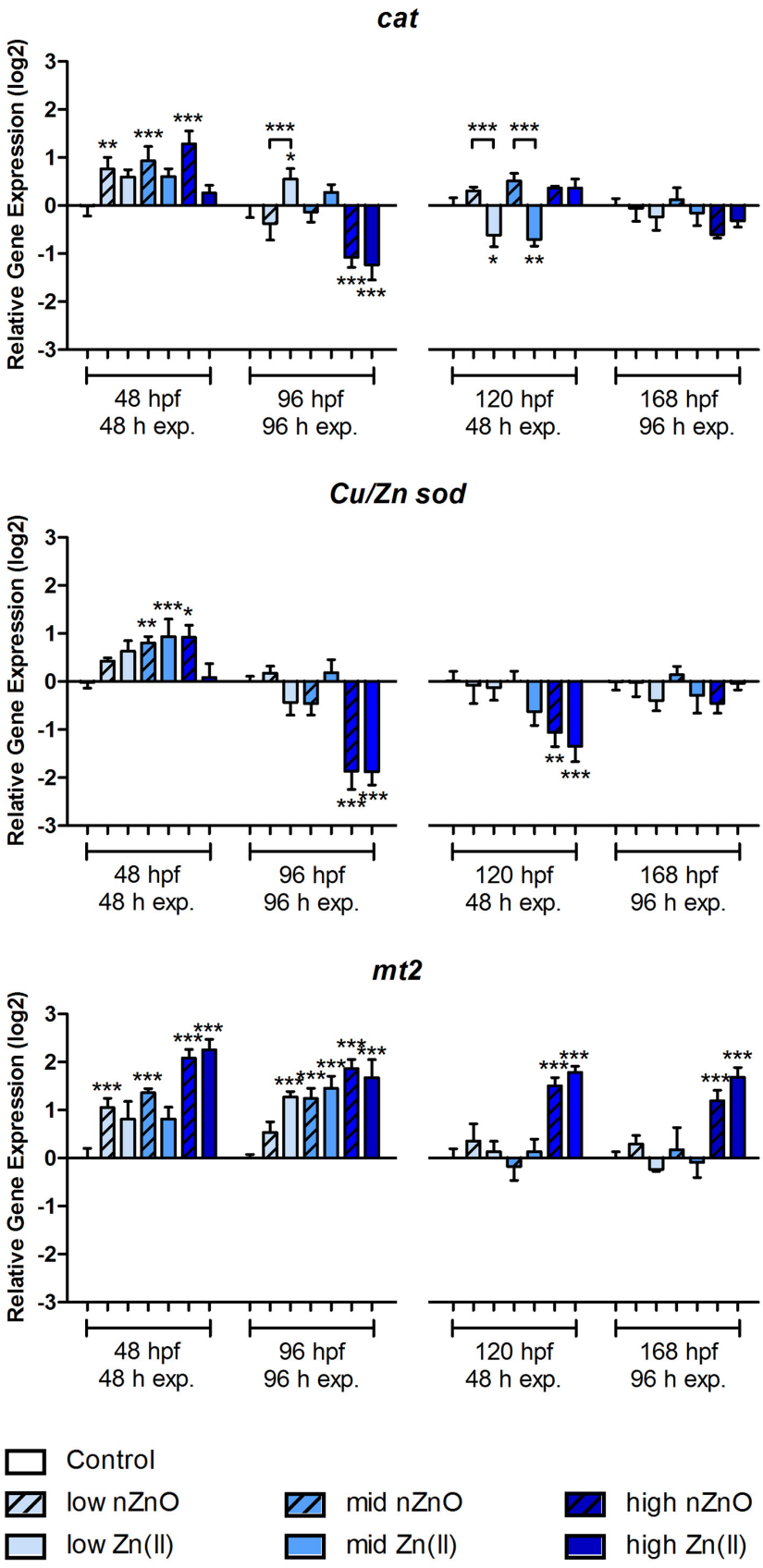
cat
Relative Gene Expression (log2)
3
2
1
0
-1
-2
-3
48 hpf
48 h exp.
96 hpf
96 h exp.
120 hpf
48 h exp.
168 hpf
96 h exp.
Cu/Zn sod
Relative Gene Expression (log2)
48 hpf
48 h exp.
96 hpf
96 h exp.
120 hpf
48 h exp.
168 hpf
96 h exp.
mt2
Relative Gene Expression (log2)
48 hpf
48 h exp.
96 hpf
96 h exp.
120 hpf
48 h exp.
168 hpf
96 h exp.
Control
low nZnO
low Zn(II)
mid nZnO
mid Zn(II)
high nZnO
high Zn(II)

Figure 6

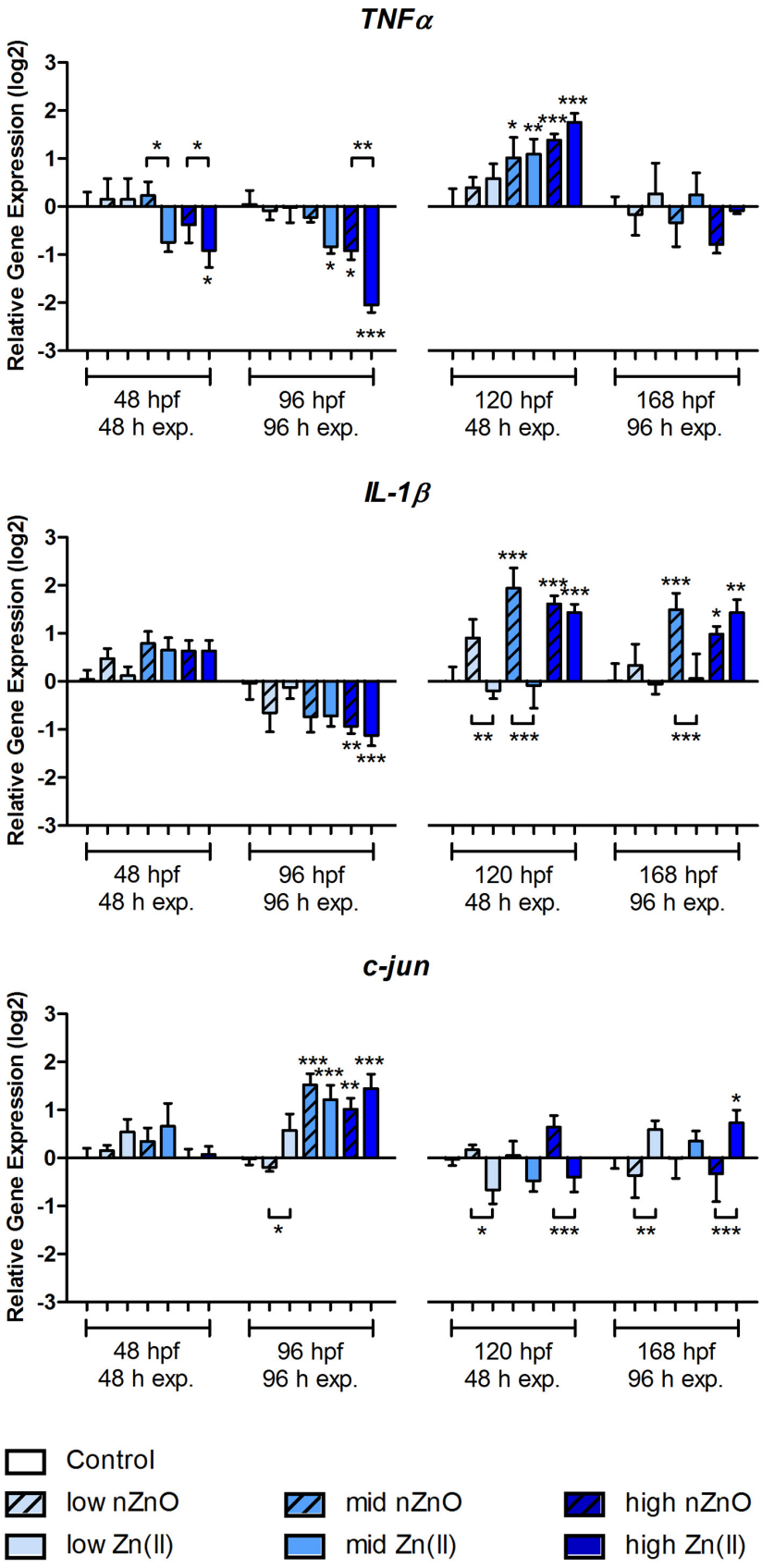
TNFα
IL-1β
c-jun
Relative Gene Expression (log2)
48 hpf
48 h exp.
96 hpf
96 h exp.
120 hpf
48 h exp.
168 hpf
96 h exp.
Control
low nZnO
low Zn(II)
mid nZnO
mid Zn(II)
high nZnO
high Zn(II)

Figure 7

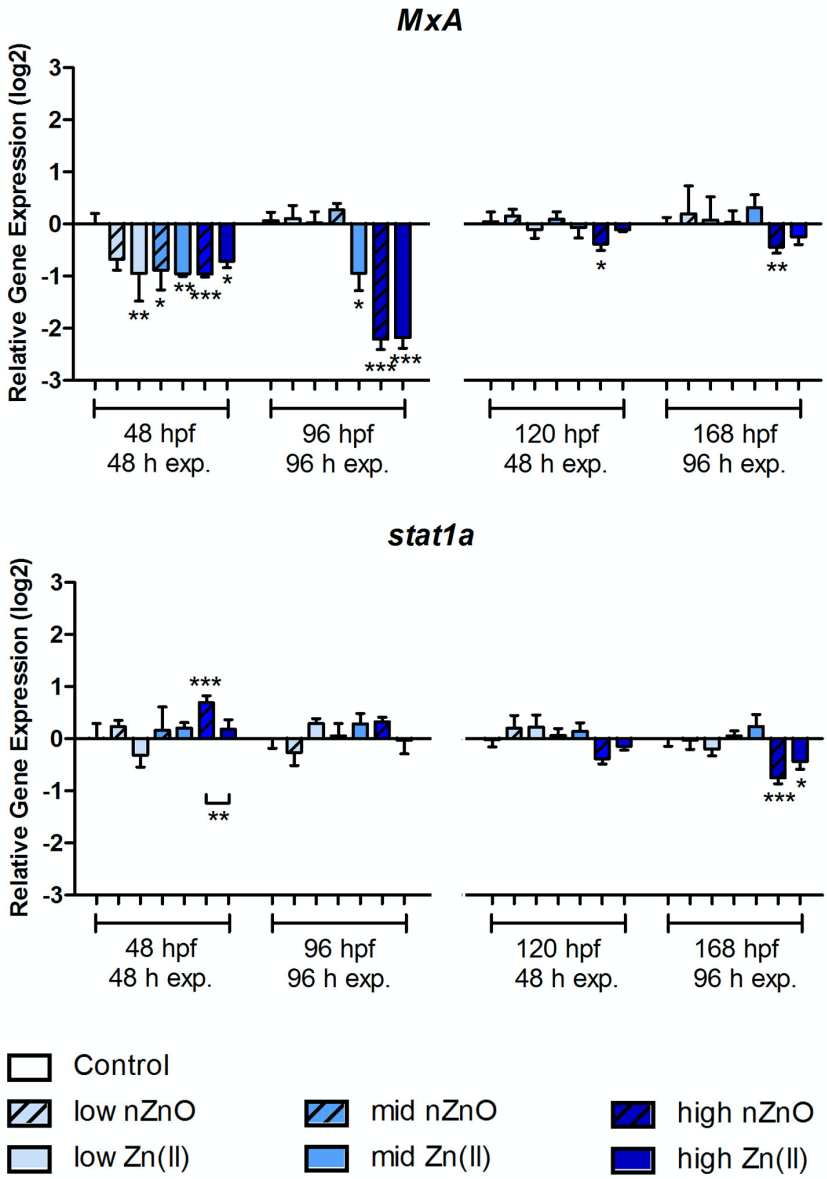
MxA
Relative Gene Expression (log2)
3
2
1
0
-1
-2
-3
48 hpf
48 h exp.
96 hpf
96 h exp.
120 hpf
48 h exp.
168 hpf
96 h exp.
stat1a
Relative Gene Expression (log2)
48 hpf
48 h exp.
96 hpf
96 h exp.
120 hpf
48 h exp.
168 hpf
96 h exp.
Control
low nZnO
low Zn(II)
mid nZnO
mid Zn(II)
high nZnO
high Zn(II)